Journal of Magnetic Resonance **146,** 157–164 (2000)
doi:10.1006/jmre.2000.2144, available online at http://www.idealibrary.com on IDEAL®

Torus Factor—The Relationship between Radiofrequency Field and Radial Position in Toroid Cavity Probes

Klaus Woelk

Institute of Physical and Theoretical Chemistry, University of Bonn, Wegelerstrasse 12, D-53115 Bonn, Germany

E-mail: woelk@thch.uni-bonn.de

Received February 9, 2000; revised June 13, 2000

Toroid detectors are resonators for high-pressure *in situ* NMR spectroscopy or one-dimensional rotating-frame imaging. One of their unique qualities is a mathematically well-defined nonuniform radiofrequency field confined to the inside of the detector. A single parameter (i.e., the torus factor) is sufficient to describe the relationship between this radiofrequency field and the radial distance from the center axis of the torus. Because accurate determination of the torus factor is essential to optimize toroid cavity NMR experiments or conduct toroid cavity imaging, a fast numerical algorithm for accurate, precise, and convenient determination of torus factors from pulse width-dependent signal intensities is introduced. In addition, the new algorithm provides for 99% confidence intervals around the refined torus factors. A computer program in which the optimization progress is visualized during the torus factor refinement is presented. Upon completion of the program, the best-fit simulated data and the residuals between best fit and experimental data are provided.

Key Words: **torus factor; toroid cavity detector; rotating-frame imaging; radiofrequency field gradient; Brent algorithm.**

INTRODUCTION

Toroid cavity probes are uniquely designed NMR probes that facilitate coaxial resonators, i.e., cylindrical TCDs (*t*oroid *c*avity *d*etectors, Fig. 1) as NMR detectors rather than conventional coil setups (e.g., solenoid or Helmholtz saddle coils). The radiofrequency field (B_1 field) of a TCD is confined to the inside of the detector (*1*); therefore, it can be mounted close to electrically conducting materials without a significant loss of inductance. Consequently, TCDs are predestined for the use in metal pressure vessels and have been utilized extensively in autoclave probes for high-pressure and high-temperature *in situ* NMR studies (*2*).

An additional, distinctive quality of TCDs is their nonuniform and mathematically well-defined radiofrequency field gradient. The B_1 field is strongest near the central conductor (Fig. 1) and drops off as the radial distance r increases (*1*)

$$B_1(r) = \frac{A}{r}, \qquad [1]$$

where A is the torus factor, i.e., the proportionality between B_1 and r^{-1}. The torus factor depends primarily on the power level of the transmitter amplifier and the quality, Q, of the probe circuitry. From Eq. [1], it is seen that a B_1 field gradient of

$$G_1(r) = \frac{dB_1(r)}{dr} = -\frac{A}{r^2} \qquad [2]$$

occurs in TCDs. In the vicinity of the central conductor, G_1 is very strong. Here, standard high-resolution NMR equipment (e.g., 100-W H-band power amplifier) is usually sufficient to generate gradients of more than 5 mT mm^{-1} (500 G cm^{-1}). Accordingly, G_1 is well suited for one-dimensional, radial RFI (*r*otating-*f*rame *i*maging) (*3*) or RFM (*r*otating-*f*rame *m*icroscopy) (*4*). Close to the central conductor, toroid-cavity RFM can resolve structures on the micrometer scale in materials that range from mobile fluids to rigid polymers. Since differences in nutation frequencies (rather than differences in Larmor frequencies) are exploited to discriminate between distances, chemical-shift information is automatically retained in RFI experiments.

Because of the nonuniform and radially dependent B_1 gradient in TCDs, accurate one-dimensional imaging is conducted only if the torus factor is known accurately and precisely. Ill-determined torus factors (i.e., determined larger or smaller than the true torus factor) lead to images in which structures appear larger or smaller than they really are. In addition, the imaged structures appear shifted on the distance axis.

In toroid-cavity MAGROFI (*m*agnetization-*g*rating *r*otating-*f*rame *i*maging), a recently developed B_1 gradient NMR technique to measure molecular diffusion (*5, 6*), the accuracy of the torus factor limits the accuracy to which a diffusion coefficient is determined. In this new technique, a single preparation pulse (P1) generates a nonuniform, radially dependent z-magnetization grating. During a subsequent evolution time τ, the grating amplitude $M_A(r)$ decays exponentially depending on the inverse of the radius to a power of 4 (*5*)

1090-7807/00 $35.00

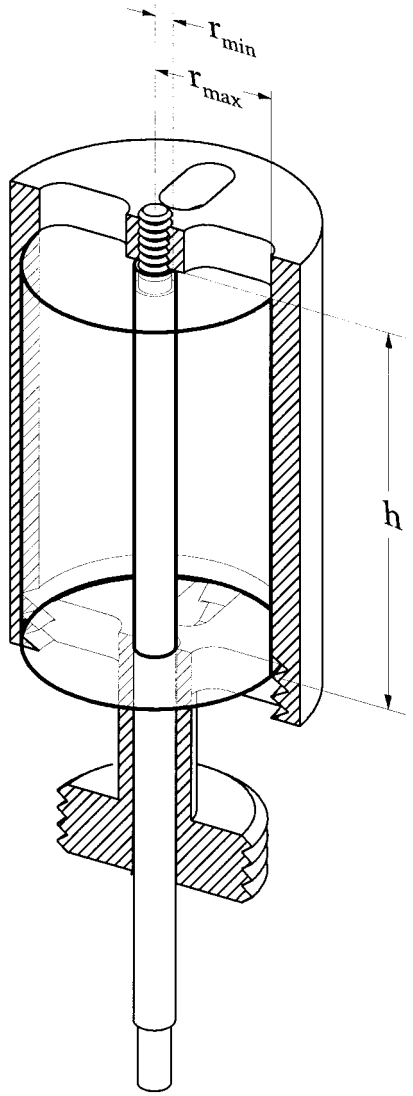

FIG. 1. Schematic drawing of a toroid cavity detector (TCD) and the enclosed sample volume. The sample volume is characterized by the inner and outer radial confines (r_{min} and r_{max}, respectively) and by the sample height (h).

$$M_A(r) = \exp\left(-\frac{D\gamma^2 A^2 t_{P1}^2 \tau}{r^4}\right), \qquad [3]$$

where D is the diffusion coefficient, γ is the magnetogyric ratio, and t_{P1} is the duration of the preparation pulse P1. As evident from Eq. [3], D and A^2 are fully interdependent. Consequently, in a fit of experimental data to the mathematical description of Eq. [3] refining the diffusion coefficient D, an error in A translates directly into an error squared in D.

Since the accuracy of the torus factor determines the accuracy to which an image is reconstructed from toroid-cavity RFI data and because torus-factor error margins govern the precision to which a diffusion coefficient is extracted from MAGROFI experiments, a fast algorithm during which the torus factor is calculated to a maximum accuracy has been developed. In addition to the calculation of the most likely torus factor, the new algorithm returns the 99% confidence interval of determination.

Any sample that is placed inside the TCD decreases its Q to some extent and also influences the value of A. Thus, a previously determined torus factor may no longer be valid if the TCD is loaded with a different sample. Consequently, the proportionality between radial distance and B_1 field in TCDs should always be determined directly from the sample under investigation. The numerical procedure introduced here serves as a fast and convenient way to conduct this determination prior to each individual TCD experiment. However, the procedure is valid only for reasonably homogeneous samples, and may not be accurate once a more complicated, nonhomogeneous sample is loaded, e.g., for imaging studies. In this case, the scaling of the radial distance axis must be conducted from known structural details of the image, such as the descent of the intensity to zero at the inner or outer sample radius of the TCD.

THEORY

The torus factor, A, is a dependent variable in the mathematical description of the RFI experiment. Accordingly, it is determined from the best fit of the mathematical description to experimental RFI data. Experimental RFI data (i.e., pulse-width-dependent signal intensities) are obtained either from conventional RFI experiments (*3*) or from the time-saving RIPT method (*r*apid *i*maging *p*ulse *t*rain) (*7–9*). After the experiment, the signal intensities are typically processed by a real Fourier transformation revealing magnetization as a function of nutation frequency, ν_1. The nutation-frequency axis is scaled by G_1 to present data on a distance axis (*1, 4*). If the B_1 gradient coil or resonator is also used as the receiving coil, Fourier-transformed intensities must be scaled appropriately to exhibit spin-concentration data as a function of distance. For example, they must be divided by r^2 in the case of TCD experiments (*1*).

Pulse-width-dependent signal intensities have been termed *pseudo-FID* (*8*) or *driven FID* (*9*). In RFI experiments, however, the attenuation of signal intensities with increasing pulse width originates almost exclusively from the interference of magnetizations of different nutation frequencies (*3, 9*), and the more appropriate term *interferogram* is used throughout this article. Interferogram intensities, $I(t)$, of homogeneously filled TCDs are mathematically described by (*1*)

$$I(t) = 2\pi h I_0 \int_{r_{min}}^{r_{max}} \sin\left(-\frac{\gamma A t}{r}\right) dr, \qquad [4]$$

where h is the sample height, r_{min} and r_{max} are the inner and outer radial sample confines, respectively (Fig. 1), and t is the

duration of the RFI pulse. The scaled intensity I_0 is independent of the radius and proportional to the spin concentration c and several NMR-console hardware parameters (e.g., the receiver gain). Because of the principle of reciprocity (*10*), I_0 is also proportional to the torus factor A_0 obtained with unit current,

$$I(t) \propto 2\pi hcA_0 \int_{r_{min}}^{r_{max}} \sin\left(-\frac{\gamma At}{r}\right) dr. \qquad [5]$$

It follows that relative interferogram intensities can be simulated by solving the integral function of radii in Eq. [5]. Because of the nutation frequency $\omega_1 = 2\pi\nu_1 = -\gamma B_1$, Eq. [1] leads to

$$r = -\frac{\gamma A}{2\pi\nu_1}, \quad \frac{dr}{d\nu_1} = \frac{\gamma A}{2\pi\nu_1^2}, \qquad [6]$$

and transforms Eq. [5] into

$$I(t) \propto \gamma hcAA_0 \int_{\nu_1(r_{min})}^{\nu_1(r_{max})} \frac{\sin(2\pi\nu_1 t)}{\nu_1^2} d\nu_1. \qquad [7]$$

The proportionalities of Eq. [7] are combined to form the amplitude b,

$$I(t) = b \int_{\nu_{max}}^{\nu_{min}} \frac{\sin(2\pi\nu_1 t)}{\nu_1^2} d\nu_1, \qquad [8]$$

where Eq. [6] was used to calculate the integration boundaries $\nu_1(r_{min}) = \nu_{1,max}$ and $\nu_1(r_{max}) = \nu_{1,min}$. From Eq. [8], pulse-width-dependent signal intensities are predicted and specific pulse widths such as the maximum-intensity or maximum-inversion pulse width are calculated. Knowing these particular pulse widths is often necessary to optimize TCD experiments (*1, 11*). Alternatively, an unknown torus factor is calculated from experimental RFI intensities, if the dependent variables A and b are refined, e.g., by a least-squares optimization. While Eq. [8] contains b explicitly, A enters into the equation through the calculation of the integration boundaries, $\nu_{1,max}$ and $\nu_{1,min}$ (Eq. [6]). Whether an unknown torus factor is calculated or a known torus factor is used to predict interferogram intensities, the integral of Eq. [8] must explicitly be solved. Unfortunately, no analytic solution is known and only series expansion or numerical solutions apply.

Solving ∫ sin(ax)/x²dx with Series Expansion

According to standard integration rules, the integral of Eq. [8] transforms into

$$\int_{\nu_{1,max}}^{\nu_{1,min}} \frac{\sin(2\pi\nu_1 t)}{\nu_1^2} d\nu_1 = \frac{\sin(2\pi\nu_{1,max} t)}{\nu_{1,max}} - \frac{\sin(2\pi\nu_{1,min} t)}{\nu_{1,min}} + 2\pi t \int_{\nu_{1,max}}^{\nu_{1,min}} \frac{\cos(2\pi\nu_1 t)}{\nu_1} d\nu_1. \qquad [9]$$

The integral cosine of Eq. [9] is solved by series expansion according to

$$\int_{\nu_{1,max}}^{\nu_{1,min}} \frac{\cos(2\pi\nu_1 t)}{\nu_1} d\nu_1 = -\ln\left(\frac{\nu_{1,max}}{\nu_{1,min}}\right) - \sum_{m=1}^{\infty} \left((-1)^m \frac{(2\pi\Delta\nu_1 t)^{2m}}{2m(2m)!}\right), \qquad [10]$$

where $\Delta\nu_1 = \nu_{1,max} - \nu_{1,min}$, and m is the index of the individual terms (a_m) of the alternating sum. The absolute values of a_m converge toward zero after the particular index $m_p \geq |\pi\Delta\nu_1 t|$ is passed. Before this, however, a_m can reach very high absolute values, and computer calculations of the sum in Eq. [10] usually fail because of severe round-off errors. For example, typical experimental parameters are $t = 8$ μs and $\Delta\nu_1 = 20$ kHz. In ^{1}H RFI ($\gamma = 26.7510 \times 10^7$ T^{-1} s^{-1}), these particular values and a typical torus factor of $A = 1$ mT mm lead to $a_5 < -10^{35}$ and $a_6 > 10^{40}$. The entire sum (Σa_m), however, is only around 10^2. Therefore, even though computer programs exist that make it possible to conduct calculations with any predetermined accuracy, a numerical analysis of the integral in Eq. [8] is preferred over series expansion.

Fast Algorithm for Numerical Integration of ∫ sin(ax)/x²dx

Nowadays, numerical integration of arbitrary functions are conventionally conducted using computer software packages like Mathematica or Maple.[1] To determine the specific integral of Eq. [8], however, a new and very fast algorithm that reduces computer calculation time by orders of magnitude compared with standard numerical integration routines is presented. Additionally, for a least-squares fit, the computation of the integral must be repeated many times, and the time saved by the new algorithm becomes significant.

The integral of Eq. [8] consists of the sine function [$\sin(2\pi\nu_1 t)$] modified by ν_1^{-2} (Fig. 2). Because of this periodic function, the integral from $\nu_{1,max}$ to $\nu_{1,min}$ is divided into several parts:

[1] Mathematica is a registered trademark of Wolfram Research, Inc., and Maple is a registered trademark of Waterloo Maple Software.

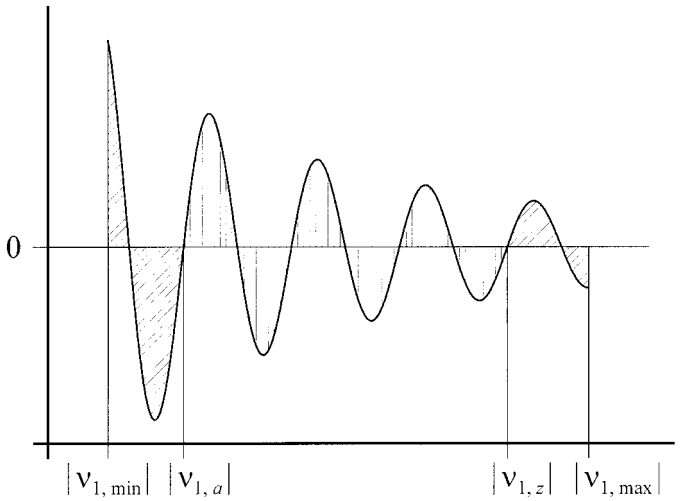

FIG. 2. Partition of the functionality of Eq. [8] into two side parts (diagonally hatched) and a center part (vertically hatched) for fast numerical integration.

$$\int_{\nu_{1,\max}}^{\nu_{1,\min}} \frac{\sin(2\pi\nu_1 t)}{\nu_1^2}\,d\nu_1 = \int_{\nu_{1,\max}}^{\nu_{1,z}} \frac{\sin(2\pi\nu_1 t)}{\nu_1^2}\,d\nu_1 + \int_{\nu_{1,z}}^{\nu_{1,a}} \frac{\sin(2\pi\nu_1 t)}{\nu_1^2}\,d\nu_1 + \int_{\nu_{1,a}}^{\nu_{1,\min}} \frac{\sin(2\pi\nu_1 t)}{\nu_1^2}\,d\nu_1. \quad [11]$$

Note that because of the convention used in Eq. [6], nutation frequencies are negative. The boundary $\nu_{1,z}$ separating the first from the second term on the right side of Eq. [11] is chosen to be the first root of the function $[\sin(2\pi\nu_1 t)]$ smaller than $[\sin(2\pi\nu_{1,\max} t)]$, which is also the start of a new sine wave period. Accordingly,

$$|\nu_{1,\max} t| \geq z > |\nu_{1,\max} t| - 1 \quad [12]$$

and $\sin(2\pi\nu_{1,z} t) = \sin(-2\pi z) = 0$. It follows that $|\nu_{1,z}| = z/t$, where z is a natural number. Similarly, the frequency $\nu_{1,a}$ separating the second from the third term on the right side of Eq. [11] is chosen to be the last root of the function $[\sin(2\pi\nu_1 t)]$ larger than $[\sin(2\pi\nu_{1,\min} t)]$, which is also the start of a new sine wave period. In analogy with the discussion above, it is found that

$$|\nu_{1,\min} t| + 1 \geq a > |\nu_{1,\min}| \quad [13]$$

and $|\nu_{1,a}| = a/t$, where a is a natural number. Figure 2 exemplifies the partition of the integral into the three distinctive parts (Eq. [11]). The two side parts ($|\nu_{1,\max}| \geq |\nu_1| \geq |\nu_{1,z}|$ and $|\nu_{1,a}| \geq |\nu_1| \geq |\nu_{1,\min}|$, respectively) are diagonally hatched, while the center part ($|\nu_{1,z}| \geq |\nu_1| \geq |\nu_a|$) is hatched vertically. Depending on pulse width, torus factor, and magnetogyric ratio the sine function of the integral in Eq. [8] may only contain one root or no root that qualifies as the start of a new sine wave period. In the first case, it is $a = z$, and the center term on the right side of Eq. [11] is equal to 0. In the second case, a partition as suggested in Eq. [11] is not possible. In both cases, the integral of Eq. [8] is calculated to a sufficient accuracy with standard routines of numerical integration (e.g., according to Simpson's rule). In all other cases, only the side parts (diagonally hatched in Fig. 2) are calculated with standard integration routines, while the center part is partitioned further according to

$$\int_{\nu_{1,z}}^{\nu_{1,a}} \frac{\sin(2\pi\nu_1 t)}{\nu_1^2}\,d\nu_1 = \sum_{k=z}^{a-1} \int_{\nu_{1,k}}^{\nu_{1,k+1}} \frac{\sin(2\pi\nu_1 t)}{\nu_1^2}\,d\nu_1, \quad [14]$$

where (similar to a and z) k is a natural number, and the relationships $|\nu_{1,k}| = k/t$ holds. With $d\nu_1/dk = -1/t$, the individual terms of the sum in Eq. [14] lead to

$$\int_{\nu_{1,k}}^{\nu_{1,k+1}} \frac{\sin(2\pi\nu_1 t)}{\nu_1^2}\,d\nu_1 = t\int_{k}^{k+1} \frac{\sin(2\pi k)}{k^2}\,dk = tS_k. \quad [15]$$

According to Eq. [15], the terms of the sum in Eq. [14] simply consist of the pulse width t times an integral, S_k, that only depends on the index k. This integral (S_k) is calculated by an appropriate numerical integration routine and tabulated for $k = 1$ to 2048 (i.e., $S_1 = 0.1033208$, $S_2 = 0.0210316$, $S_3 = 0.0075449$, ..., $S_{2048} = 3.76320 \times 10^{-11}$). With increasing index, S_k approaches zero, and terms with $k > 2048$ are so small that they can be neglected in a calculation of the integral of Eq. [11] according to

$$\int_{\nu_{1,\max}}^{\nu_{1,\min}} \frac{\sin(2\pi\nu_1 t)}{\nu_1^2}\,d\nu_1 = \int_{\nu_{1,\max}}^{\nu_{1,z}} \frac{\sin(2\pi\nu_1 t)}{\nu_1^2}\,d\nu_1 + \int_{\nu_{1,a}}^{\nu_{1,\min}} \frac{\sin(2\pi\nu_1 t)}{\nu_1^2}\,d\nu_1 + t\sum_{k=z}^{a-1} S_k. \quad [16]$$

Because the center term of Eq. [11] (vertically hatched area in Fig. 2) typically covers most of the nutation frequencies inside the TCD (except when t is very small), a computer calculation that follows the integral partition of Eq. [16] using tabulated values for S_k is many times faster than using conventional integration routines for the entire integral. If, for example, Simpson's rule is employed as an integration routine, at least 12 equally spaced data points per sine wave are needed to keep numerical calculation errors reasonably small (below 1%). In addition to the determination of these 12 data points, their function values must each be calculated according to the inte-

gral argument of Eq. [8]. This argument involves a sine function, a division, and a square calculation. Furthermore, each value is multiplied by a coefficient and all values must be added. Since, in computer calculations, a sine function itself is calculated from the sum of many terms of a series expansion, the calculation of the integral of a single sine wave period easily consists of 500 individual calculation steps. Using Eq. [16], however, this calculation is substituted simply by the access to a stored value. Accordingly, the new procedure is at least 500 times faster for each sine wave period that must be calculated.

DETERMINING THE TORUS FACTOR

With the magnetogyric ratio (γ) of the nucleus under investigation, the geometric parameters of the TCD sample volume ($r_{\min}$ and $r_{\max}$), and the experimental parameters i and Δt, where i is the number of increments of pulse width Δt (i.e., $t = i\Delta t$), Eq. [8] is used to refine an unknown torus factor by nonlinear regression. For each refined guess of A, the boundaries $\nu_{1,\max}$ and $\nu_{1,\min}$ are determined with Eq. [6], and relative intensities $I_{i,\mathrm{sim}}$ are calculated from the integral of Eq. [16]. The index i indicates the number of pulse width increments Δt that have been used to obtain the experimental intensity $I_{i,\mathrm{exp}}$. After the calculation of the relative intensities $I_{i,\mathrm{sim}}$, the scaling factor b is optimized to match the experimental data, $I_{i,\mathrm{exp}}$. Arbitrary scaling leads to

$$I_{k,\mathrm{exp}} = bI_{k,\mathrm{sim}} + \epsilon_k, \qquad [17]$$

where ϵ_k is the deviation between experimental and scaled, simulated intensity of data point k. Optimum scaling, however, is achieved, when the sum of all deviations squared is minimal. Accordingly,

$$\frac{d\sum_{k=1}^{n}\epsilon_k^2}{db} = 0, \quad \frac{d^2\sum_{k=1}^{n}\epsilon_k^2}{db^2} > 0. \qquad [18]$$

From substitution of Eq. [17] into Eq. [18], optimum scaling is given by

$$b = \frac{\sum_{k=1}^{n}(I_{k,\mathrm{exp}}I_{k,\mathrm{sim}})}{\sum_{k=1}^{n}I_{k,\mathrm{sim}}^2}. \qquad [19]$$

To refine the torus factor A in a nonlinear regression, the minimum of the so-called χ^2 parameter with respect to the dependent variable A is used as the maximum-likelihood criterion

$$\chi^2 = \sum_{i=0}^{n-1}\left(\frac{I_{i,\mathrm{exp}} - bI_{i,\mathrm{sim}}}{\sigma_i}\right)^2, \qquad [20]$$

where σ_i is the experimental standard deviation of data point i. A well-known iterative procedure to minimize χ^2 is the Levenberg–Marquardt algorithm (*12*). This algorithm, however, requires partial derivatives that are unknown for the functionality of Eq. [8] and that would need to be approximated during the iterative procedure. Consequently, the one-dimensional approach developed by Brent (*13*) calculating a minimum without derivatives is preferred in torus-factor determinations. Brent's algorithm is found as computer-code subroutine in the literature (*14b*) and finds a minimum confidently, if the minimum is unambiguously bracketed between two known values.

Experience shows that the χ^2 parameter (Eq. [20]) runs through a single minimum when the torus factor is successively increased in interferogram simulations, starting with $A \approx 0$ (*15*). Brent's algorithm speeds up the determination of this minimum but requires three consecutive starting parameters (A_a, A_b, and A_c), where the best-fit parameter (A_{opt}) is bracketed between A_a and A_c. In addition, the function value $\chi^2(A_b)$ must be smaller than the function values of $\chi^2(A_a)$ and $\chi^2(A_c)$ (*14b*). These requirements are most confidently fulfilled if the following starting values are selected

$$A_a = 0.5A_b,$$
$$A_b = \frac{\pi(2r_{\min} + r_{\max})}{6\gamma t_{\max}},$$
$$A_c = 1.5A_b, \qquad [21]$$

where $t_{\max}$ is the experimentally determined maximum-intensity pulse width (*1*). The starting value A_b in Eq. [21] is likely to be already very close to the optimized torus factor A_{opt} and easily calculated from geometric and experimental TCD parameters. Its equation is derived from a radiofrequency field (B_1') for which the 90° pulse width coincides with the TCD's maximum-intensity pulse width ($t_{\max}$). Accordingly,

$$\gamma B_1' t_{\max} = \frac{\pi}{2}. \qquad [22]$$

In addition, B_1' is assumed to occur at a radial distance, $r(A_b)$, one-third between $r_{\min}$ and $r_{\max}$:

$$r(A_b) = \frac{2r_{\min} + r_{\max}}{3}. \qquad [23]$$

With $B_1' = A_b/r(A_b)$, Eqs. [22] and [23] lead to the starting value of A_b in Eq. [21].

Figure 3 exhibits the result of refining A and b according to Brent's approach and Eq. [19], respectively. The upper plot compares experimentally derived interferogram intensities (circles) with data calculated from the best-fit parameters (solid line). The experimental intensities were obtained with ^{1}H NMR

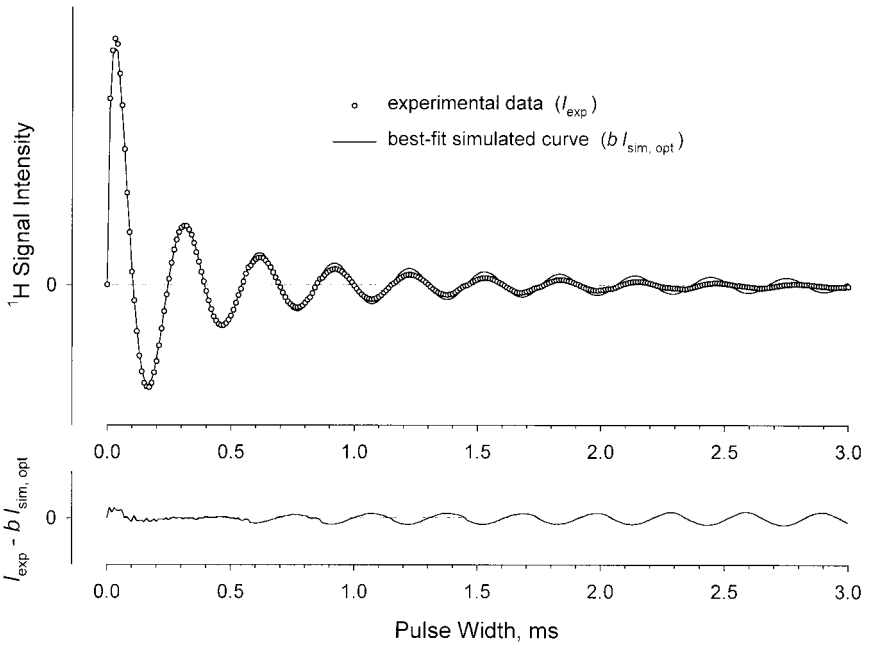

FIG. 3. Plot of experimental interferogram intensities (200 MHz, ^{1}H NMR) as a function of pulse width (open circles, upper plot) obtained from a TCD (r_{min} = 0.7 mm, r_{max} = 8.5 mm) completely filled with a solution of 10% chloroform in acetone-d_6. The data are compared to the best fit of Eq. [8] (solid line, upper plot) after refining the torus factor and optimally scaling the intensities. The residual intensities between experimental and simulated data are shown as a solid line in the lower plot.

(200 MHz, 50-W observe transmitter) from a TCD filled with a solution of 10% chloroform in acetone-d_6 (r_{min} = 0.7 mm and r_{max} = 8.5 mm). In particular, integrated intensities of the ^{1}H chloroform signals derived from 512 spectra with incrementally increasing pulse width (pulse width increment of dt = 10 μs) are plotted as a function of pulse width (t). The best-fit torus factor (A_{opt} = 0.6138 mT mm) that leads to the simulated curve in Fig. 3 indicates nutation frequencies between ν_{max} = 37.3 kHz at r_{min} and ν_{min} = 3.1 kHz at r_{max} (Eq. [6]). The lower plot of Fig. 3 shows the residuals between experimental and simulated data, which are not purely statistic (i.e., not only consist of noise) but contain oscillations that coincide with the oscillations of the interferogram. These oscillations arise from experimental intensities decaying faster than calculated by interference of nutation frequencies only (simulated curve). This additional decay originates from relaxation or diffusion during the pulses of the RFI experiment. While both effects have been neglected in the derivation of Eq. [8], they must be considered in a complete analysis of RFI experiments. However, including relaxation as a dependent parameter in the calculation, for example, led to the same best-fit torus factor and did not improve the confidence to which the torus factor is determined.

99% CONFIDENCE OF TORUS-FACTOR DETERMINATION

The confidence to which a dependent parameter is obtained from refinement procedures is usually indicated by a region (confidence interval) around the best-fit parameter, in which the true parameter is found to a certain confidence (e.g., 99% confidence). In standard computer routines, these intervals are calculated from gradient and curvature matrix elements (i.e., from partial derivatives). In torus-factor optimizations, however, Brent's algorithm without derivatives is preferred and confidence intervals are also determined without derivatives.

For confidence-interval calculations, it is essential to either know the experimental standard deviations of interferogram intensities (σ_i in Eq. [20]) or to estimate them from the quality of the best-fit simulation (*14c*). For the latter, standard deviations are initially set to unity ($\sigma_i = \sigma_0 = 1$) and recalculated after the minimum χ^2 is found according to

$$\sigma_0^2 = \frac{\sum_{i=0}^{n-1} (I_{i,\mathrm{exp}} - bI_{i,\mathrm{sim,opt}})^2}{n - l}, \qquad [24]$$

where $I_{i,\mathrm{sim,opt}}$ are the optimized, simulated relative intensities, and l is the number of dependent parameters varied to obtain the minimum χ^2 (Eq. [20]). Because only the torus factor is varied to minimize χ^2, the number of dependent variables in Eq. [24] is $l = 1$. For comparison, the scaling factor b is separately optimized using Eq. [19] and, thus, not dependent in the determination of the minimum χ^2. With the standard deviation σ_0 of Eq. [24], the minimum χ^2 is recalculated (Eq. [20]) to give the meaningful, absolute value χ^2_{min}. With χ^2_{min}, the 99% confidence interval for $l = 1$ is defined (*14c*) as the region $\pm\Delta A$ around A_{opt} for which

$$\chi^2 \leq \chi^2_{\min} + 6.63. \quad [25]$$

Assuming that this region is symmetric around A_{opt}, it is sufficient to determine only one of the two points of intersection between the χ^2 curve and the threshold given by Eq. [25]. The point of intersection is calculated by the secant method that numerically determines the root of a smoothly curved functionality. The secant method is found as computer-code subroutine in the literature (*14a*) and is preferred over other methods (e.g., *regula falsi*) for it finds a root even if it is not unambiguously bracketed between two known values. To obtain the threshold of Eq. [25] as root, all χ^2 values used for the secant calculation are diminished by ($\chi^2_{\min} + 6.63$). Two starting values are required, one of which should be positive and the other negative. The negative starting value is easily obtained from $\chi^2_{\min}$ that is always below the threshold of Eq. [25] (i.e., negative with respect to the threshold). The χ^2 value of $A = 1.01\ A_{opt}$ is, in most cases, already above the threshold. Accordingly, for example, the secant method leads to a 99% confidence interval of $\Delta A = \pm 0.0017$ mT mm for the experiment in Fig. 3 (i.e., $\Delta A = \pm 0.3\%$ with respect to $A_{opt} = 0.6138$ mT mm). For many TCD experiments, the 99% confidence to which the torus factor is determined is below $\pm 1\%$. Again, this shows that the simple description of the B_1 field in TCDs (Eq. [1]) is very accurate and RFI/RFM in TCDs is conducted to a high precision.

COMPUTER PROGRAM FOR TORUS-FACTOR DETERMINATION

Because of the importance of accurate and confident determination of torus factors for TCD spectroscopy and imaging, a fast computer program was developed and is available from the author upon request.

The program performs the following procedures and routines: first, an input routine asks for the inner and outer sample confines (r_{min} and r_{max}, respectively), the pulse width increment (Δt), the nucleus under investigation, and the name of the RFI-intensity data file containing an arbitrary number of experimental intensities $I_{i,exp}$ as a list of values. From the input parameters, starting values of the Brent algorithm are calculated according to Eq. [21], and interferogram intensities ($I_{i,sim}$) are calculated according to the fast numerical integration routine described above. The experimental pulse widths ($t = i\Delta t$) are used for the integration routine, so that simulated intensities ($I_{i,sim}$) occur at the same points of the time axis as those of the experimental data. With $I_{i,exp}$ and $I_{i,sim}$, the optimum scaling factor (b) is calculated according to Eq. [19], and the sum of deviations squared is determined from Eq. [20] with experimental standard deviations σ_i set to unity.

With Brent's algorithm, the minimum χ^2 is determined iteratively to an accuracy in the range of the computer's roundoff error. Thereafter, the standard deviation is recalculated according to Eq. [24] and the minimum χ^2 calibrated to give $\chi^2_{\min}$. At last, the 99% confidence interval is determined using the numerical secant method described above.

To follow the optimization progress during the calculations, experimental and simulated data are visualized on the monitor as a plot of intensities versus pulse width similar to that in Fig. 3. The simulation is updated every time a better fit is found. In addition, residuals between experiment and simulation are shown and updated in a separate plot.

The program code uses the routines "BRENT" (*14b*) and "RTSEC" (*14a*) from the literature. The iterative calculation is usually finished after a few seconds, even though three different numerical routines are executed many times. The original source code was written in Pascal and compiled into a executable computer program using Turbo Pascal 5.5.[2] The program uses two additional data files. The first contains magnetogyric ratios of all known NMR-active isotopes (*16*), while the second contains precalculated values of S_k ($k = 0, 1, 2, \ldots, 2048$) used in the calculation of the integral of Eq. [16]. Upon leaving the program, the best-fit simulated data and the residuals are saved in a separate data file for further use or analysis.

ACKNOWLEDGMENTS

The author thanks E. Lehnhof, University of Bonn, for providing many sets of experimental RFI data (*15*), P. Trautner, University of Bonn, for carefully reviewing the computer program source code, R. E. Gerald II, Argonne National Laboratory, for testing the program, and R. J. Klingler, Argonne National Laboratory, for the suggestion to add the plot of residuals to the display of experimental and simulated data.

REFERENCES

1. K. Woelk, J. W. Rathke, and R. J. Klingler, The toroid cavity NMR detector, *J. Magn. Reson. A* **109,** 137–146 (1994).
2. J. W. Rathke, R. J. Klingler, R. E. Gerald II, K. W. Kramarz, and K. Woelk, Toroids in NMR spectroscopy, *Prog. NMR Spectrosc.* **30,** 209–253 (1997).
3. D. I. Hoult, Rotating frame Zeugmatography, *J. Magn. Reson.* **33,** 183–197 (1979).
4. K. Woelk, J. W. Rathke, and R. J. Klingler, Rotating-frame NMR microscopy using toroid cavity detectors, *J. Magn. Reson. A* **105,** 113–116 (1993).
5. K. Woelk, R. E. Gerald II, R. J. Klingler, and J. W. Rathke, Imaging diffusion in toroid cavity probes, *J. Magn. Reson. A* **121,** 74–77 (1996).
6. K. Woelk, B. L. J. Zwank, J. Bargon, R. J. Klingler, R. E. Gerald II, and J. W. Rathke, Imaging diffusion with non-uniform B_1 gradients, *in* "Spatially Resolved Magnetic Resonance" (B. Blümich, P. Blümler, R. Botto, and E. Fukushima, Eds.), pp. 103–110, Wiley–VCH, Weinheim (1998).
7. K. R. Metz and J. P. Boehmer, Technique for rapid rotating-frame imaging, *Magn. Reson. Imaging* **6** (Suppl. 1), 53 (1988).
8. D. Boudot, D. Canet, and J. Brondeau, Spatial labeling by a radiofrequency field gradient. DANTE-Z profile, probed by one-dimensional nutation imaging, *J. Magn. Reson.* **87,** 385–394 (1990).

[2] Turbo Pascal is a registered trademark of Borland International, Inc.

9. K. R. Metz, J. P. Boehmer, J. L. Bowers, and J. R. Moore, Rapid rotating-frame imaging using an RF pulse train (RIPT), *J. Magn. Reson. B* **103,** 152–161 (1994).

10. D. I. Hoult and R. E. Richards, The signal-to-noise ratio of the nuclear magnetic resonance experiment, *J. Magn. Reson.* **24,** 71–85 (1976).

11. K. Woelk and J. W. Rathke, Composite 90° and 180° pulses to compensate for radiofrequency gradients in toroid NMR detectors, *J. Magn. Reson. A* **115,** 106–115 (1995).

12. D. W. Marquardt, An algorithm for least squares estimation of nonlinear parameters, *J. Soc. Industr. Appl. Math.* **11,** 431–441 (1963).

13. R. P. Brent, "Algorithms for Minimization without Derivatives," Chap. 5, Prentice–Hall, Englewood Cliffs, NJ (1973).

14. W. H. Press, S. A. Teukolsky, W. T. Vetterling und B. P. Flannery, "Numerical Recipes in C—The Art of Scientific Computing," 2nd ed., (*a*) pp. 354–357, (*b*) pp. 404–405, and (*c*) pp. 683–697, Cambridge Univ. Press, Cambridge, UK (1992).

15. E. Lehnhof, "Bestimmung des Torusfaktors für die Nutationsbildgebung im Torus-Hohlraumdetektor," Thesis (Diplomarbeit), University of Bonn, Germany, 1997.

16. NMR Frequency Table, *in* "Tables and Other Useful Information," Bruker Almanac, pp. 2–7, Bruker Analytik, Karlsruhe (1997).